Performance evaluation of sandwich detector-based CT

Seungwoo Ha [a], Dong Woon Kim [a], Junwoo Kim [a], Ho Kyung Kim[a,b*]
[a]*School of Mechanical Engineering, Pusan National University, Busan, Republic of Korea*
[b]*Center for Advanced Medical Engineering Research, Pusan National University, Busan, Republic of Korea*
[*]*Corresponding author: hokyung@pusan.ac.kr*

1. Introduction

Dual-energy computed tomography (DECT) has the advantage in the discrimination of materials in objects and this could raise the conspicuity of target materials in complex structure, due to the elimination of non-interest materials [1,2,3]. However, dual-shot DE technique, such as kVp switching and dual-source CT, may cause the motion artifacts in DE images because of time-delay in x-ray exposure. For the motion artifact-free DECT, single-shot DECT using a multi-layer detector, or sandwich detector, can be adapted.

The sandwich detector consists of three layers: an inter-layer filter, a front layer, and a rear layer. The inter-layer filter can make the sandwich detector achieve spectral separation, using beam hardening effect. The front and rear layers collect x-ray photons for different x-ray spectrum, simultaneously, which enables the time delay to disappear. However, the front detector and the inter-layer filter reduce the number of x-ray photons reaching the rear detector, which may affect the system performances. In order to design the sandwich detector, a quantitative analysis will be conducted as changing the thickness of the inter-layer filters.

2. Materials and Methods

2.1 Sandwich detector

Figure 1 is the sketch of the sandwich detector, consisting of a thin phosphor coupled front detector, a beam-hardening inter-layer copper filter and a thick phosphor coupled rear detector. The inter-layer filter makes it possible for the front and rear detector to have different x-ray spectrum shapes with a different mean energy by beam-hardening effect. Using two energies, the sandwich detector is able to perform the log-subtraction method as a DE imaging technique [4].

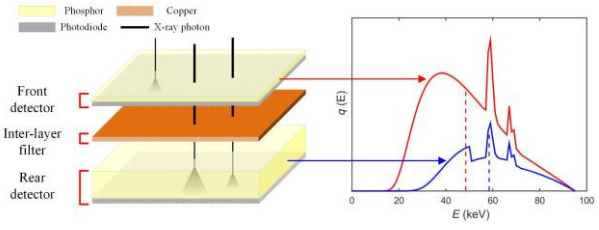

Fig. 1. The sketch of the sandwich detector and the spectrum shapes of a thin phosphor coupled front detector and a thick phosphor coupled rear detector.

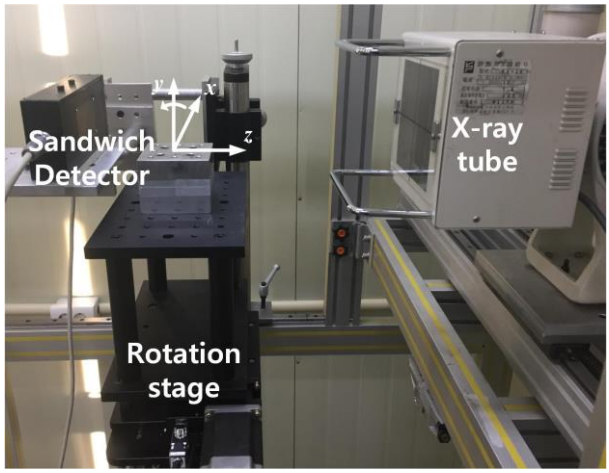

Fig. 2. The system of sandwich CT. The x-ray tube, the sandwich detector, and the rotation stage mainly compose the CT system.

2.2 Sandwich CT system

The sandwich CT system mainly consists of an x-ray tube, a sandwich detector, and a rotation stage, as shown in figure 2. The tube voltage is set as 95 kVp and the tube current as 0.64 mAs per a projection image. The detector has the pixel pitch of 0.048 mm and the pixel format of 1024×1000, which means the active area of the detector is approximately 50×25 cm^2.

2.3 Quantitative performance evaluation

To evaluate the quantitative performances of the sandwich detector, three kinds of indices are adapted: the modulation transfer function (MTF) for a resolution performance, the noise-power spectrum (NPS) for a noise performance, and the noise-equivalent number of quanta (NEQ) for a system performance [5,6,7].

For the measurement of the MTF, a tungsten wire phantom (QRM-MicroCT-Wire, QRM GmbH, Germany) with a diameter of 0.025 mm is used. Figure 3 shows the flow of MTF measurement. The reconstructed tungsten wire images are projected along the specific direction, which means applying Radon transform to the 3D image, to obtain 2D slit-like image. Then, using projected slit-like image, a fine-sampling is conducted on the image for the acquisition of the line-spread functions (LSFs). Finally, the MTFs are calculated by applying the fast Fourier transform (FFT) to the LSFs.

The NPS measurement employs a water cylinder phantom (QRM-MicroCT-Water, QRM GmbH, Germany) with a diameter of 33mm and a height of 66 mm. Figure 4 shows the flow of NPS measurement. Several volumes of interest (VOIs) are selected from the reconstructed water images, and used for the calculation of the volumetric NPS by applying 3D FTT to the average noise value of VOIs. After extracting central slice of volumetric NPS, the averaged extraction is conducted on the planar NPS along f_r direction for the acquisition of 1D NPS.

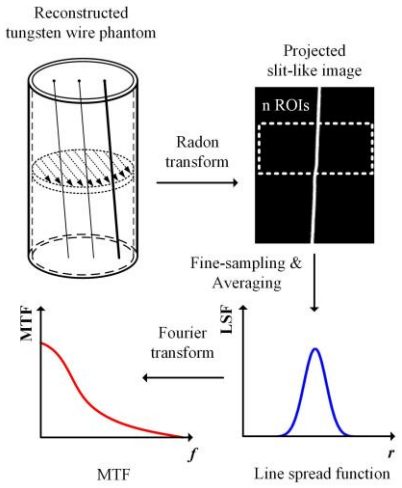

Fig. 3. The flow of MTF measurement. The reconstructed tungsten wire phantom is projected for the acquisition of slit-like image. After fine-sampling and averaging slit-like image for LSFs, Fourier transform is conducted on the LSFs to obtain MTF.

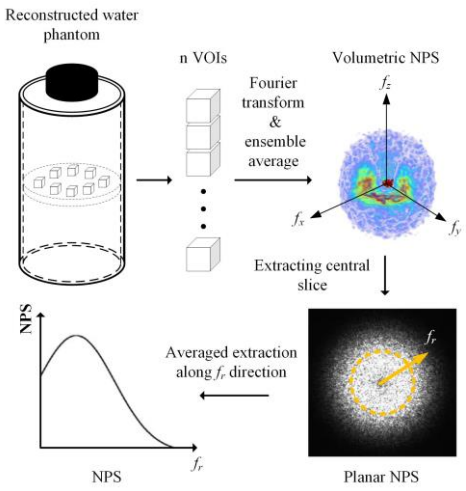

Fig. 4. The flow of NPS measurement. The VOIs are selected from the reconstructed water cylinder and 3D FFT and ensemble averaging are applied to them for the acquisition of volumetric NPS. The central slice of 3D NPS is extracted and averaged along f_r direction to obtain the NPS.

The NEQ means the image quality of the real CT system compared to the ideal CT system. The NEQ can be calculated by the MTF and NPS. The square of the MTF multiplied by the radial sampling density, πf , and divided by the NPS is the NEQ.

3. Preliminary results

Figure 5 shows the MTF, NPS, and NEQ performances when the 0.1 mm copper filter is selected as the inter-layer filter.

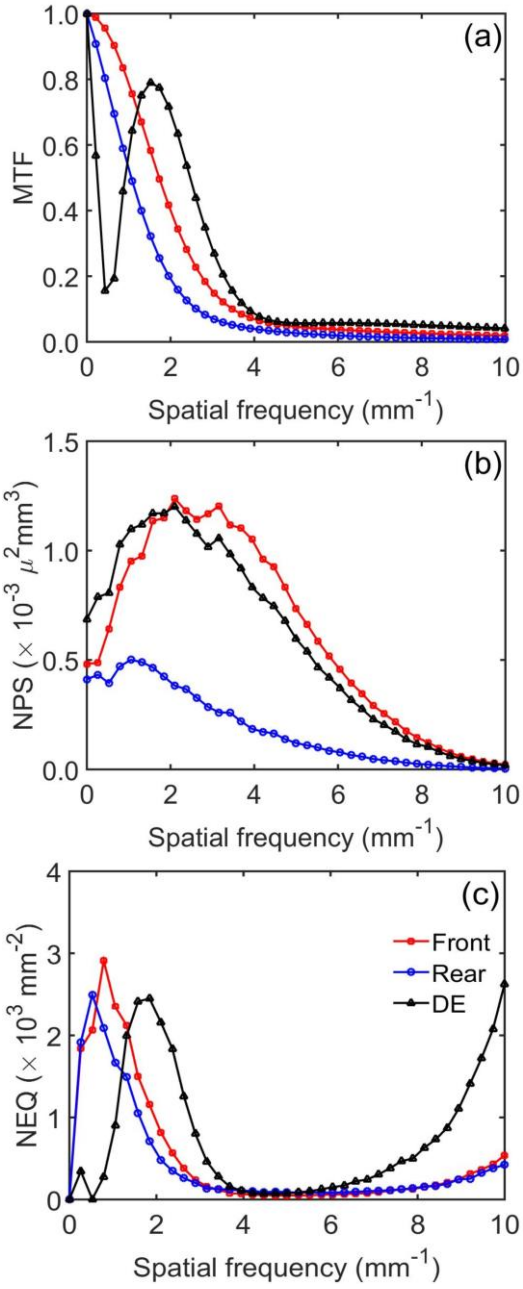

Fig. 5. The quantitative performances for the front, rear, and DE system. (a) The MTF, (b) NPS, and (c) NEQ results are plotted at 0.1 mm copper filter.

In the case of the MTF, the front CT system shows better performance than the rear CT system. It is because the front detector is coupled with a thin phosphor which narrowly spreads light photons, and the rear detector with a thick phosphor, widely spreading light photons. The difference of the MTFs between CT systems makes a unique MTF shape in DECT system, which means the DECT could enhance the edge in specific spatial frequency.

The NPS result shows that the front system has higher noise than the rear one. Although the number of x-ray photons reaching the rear phosphor is lower than that of the front one, the quantum efficiency of the rear phosphor is higher than that of the front one because of thick phosphor in the rear one. This results the lower NPS in the rear system than the front system.

The NEQ performances in front and rear system show similar graph shapes, which means that the front and the rear CT system have little difference in the NEQ. In the case of the DECT system, it shows the shifted NEQ graph. This means the DECT system could enhance objects in the specific spatial frequency.

4. Further study

To see the effect of the inter-layer filter thickness, various thicknesses will be used for the further study. In addition, the tendency of the performances will be examined.

ACKNOWLEGMENTS

This work was supported by the National Research Foundation of Korea (NRF) grants funded by the Korea government (MSIP) (No. 2017M2A2A6A01019930)

REFERENCES

[1] R. Alvarez and A. Macovski, Energy-selective reconstructions in X-ray computerized tomography, Physics in Medicine and Biology, Vol.21, pp. 733-744, 1976.
[2] D. Xu, D. A. Langan, X. Wu, J. D. Park, T. M. Benson, J. Tkaczky, and A. M. Schmitz, Dual energy CT via fast kVp switching spectrum estimation, in Proc. SPIE, Vol. 7258, P. 72583T, 2009.
[3] T. R. Johnson, B. Karuß, M. Sedlmair, M. Grasruck, H. Bruder, D. Morhard, C. Fink, S. Weckbach, M. Lenhard, B. Schmidt, T. Flohr, M. F. Reiser, and C. R. Becker, Material differentiation by dual-energy CT: initial experience, Eur. Radiol, Vol. 17, pp. 1510-1517, 2007.
[4] S. Richard, J. H. Siewerdsen, D. A. Jaffray, D. J. Moseley, and B. Bakhtiar, Generalized DQE analysis of radiographic and dual-energy imaging using flat-panel detectors, Med. Phys., Vol. 32, pp. 1397-1413, 2005.
[5] H. Watanabe, E. Honda, and T. Kurabavashi, Modulation transfer function evaluation of cone beam computed tomography for dental use with the oversampling method, Dentomaxillofac. Rad. Vol. 39, pp. 28-32, 2000.
[6] J. H. Siewerdsen, I. A. Cunningham, and D. A. Jaffray, A framework for noise-power spectrum analysis of multidimensional images, Med. Phys., Vol. 29, pp. 2655-2671, 2002.
[7] D. J. Tward, and J. H. Siewerdsen, Noise aliasing and the 3D NEQ of flat-panel cone-beam CT: Effect of 2D/3D apertures and sampling, Med. Phys., Vol. 36, pp. 3830-3843, 2009.